

Erosion susceptibility mapping of a loess-covered region using Analytic Hierarchy Process – A case study: Kalat-e-Naderi, northeast Iran

FATEMEH NOOSHIN NOKHANDAN¹, KAVEH GHAHRAMAN¹ and ERZSÉBET HORVÁTH¹

Abstract

In this study, the Analytic Hierarchy Process (AHP) is applied to generate erosion susceptibility maps in four basins of Kalat-e-Naderi county, namely Archangan, Kalat, Qaratigan, and Chahchaheh basins, situated in northeast Iran. The Kalat-e-Naderi region is characterized by a partial coverage of loess. Given the agricultural significance of loess and its susceptibility to erosion, this research focuses specifically on regions covered by loess. Geographic Information System (GIS) tools, including ArcMap and Quantum Geographic Information System (QGIS), were utilized to facilitate the creation of erosion susceptibility maps. Seven factors, including slope, aspect, elevation, drainage density, lithology, the Normalized Difference Vegetation Index (NDVI), and precipitation were selected for consideration. Recognizing the variability of precipitation and vegetation cover across different seasons, seasonal data for the specified factors were employed. Consequently, erosion susceptibility maps were generated on a seasonal basis. Pairwise comparison tables revealed that precipitation, lithology, and slope emerged as the dominant factors contributing to erosion susceptibility in this region. The resultant maps distinctly delineate basins with higher precipitation values, unresistant lithology (such as loess, characterized by high porosity and permeability), and steeper slopes, exhibiting heightened susceptibility to erosion (Archangan and Kalat basins). The credibility of the research findings was examined through on-site observations. The outcomes of this study may provide pertinent insights for decision-makers and planners. This information can be effectively employed in formulating strategies aimed at conserving soil quality in areas vulnerable to erosion hazards.

Keywords: Analytic Hierarchy Process (AHP), erosion susceptibility on loess, GIS, Kalat-e-Naderi

Received July 2023, accepted November 2023.

Introduction

Soil erosion stands as a critical global environmental challenge, exerting far-reaching impacts on agricultural productivity, natural resources, and socio-economic development (JEBUR, M.N. *et al.* 2014; ZHAO, J. *et al.* 2016; LI, Y. *et al.* 2020; VANMAERCKE, M. *et al.* 2021; CEN, Y. *et al.* 2022). Soil erosion is speeded up by a complex interplay of environmental factors, such as topography, soil characteristics, climate, and vegetation, as well as human activities like deforestation, farming,

and construction (LUKIĆ, T. *et al.* 2018, 2019; THOMAS, J. *et al.* 2018; ABBAS, S. *et al.* 2022). To mitigate soil erosion, diverse strategies, ranging from conservation tillage to the implementation of hydraulic structures, have been developed (MORGAN, R. 1995; BARBERA, V. *et al.* 2012; LUKIĆ, T. *et al.* 2016). Due to the importance of soil erosion, researchers have been investigating soil erosion using different models, including Agricultural Non-point Source Pollution Model (AGNPS) (YOUNG, R. *et al.* 1989; ZHU, K.-W. *et al.* 2020; ZOU, L. *et al.* 2020; HUANG, C. *et al.* 2022), Soil and Water

¹ Department of Physical Geography, ELTE Eötvös Loránd University, Pázmány Péter sétány 1/C, H-1117, Budapest, Hungary. E-mails: fatimanooshin@gmail.com, kevingh70@gmail.com, erzsebet.horvath@ttk.elte.hu

Assessment Tool (SWAT) (NEITSCH, S.L. *et al.* 2011; BHATTACHARYA, R.K. *et al.* 2020; ECHOGDALI, F.Z. *et al.* 2022), European Soil Erosion Model (EUROSEM) (MORGAN, R. *et al.* 1998; PANDEY, S. *et al.* 2021; RAZA, A. *et al.* 2021; SHEN, N. *et al.* 2023), Erosion Potential Model (EPM) (AHMADI, M. *et al.* 2020; ENNAJI, N. *et al.* 2022; ALEKSOVA, B. *et al.* 2023), and Revised Universal Soil Loss Equation (RUSLE) (KEBEDE, Y.S. *et al.* 2021; ASWATHI, J. *et al.* 2022; MICIĆ PONJIGER, T. *et al.* 2023). Besides the mentioned methods, the AHP (SAATY, T.L. 1980) is widely used to investigate soil erosion and to map the erosion susceptible areas (SAHA, S. *et al.* 2019; DAS, B. *et al.* 2020; KUCUKER, D.M. and GIRALDO, D.C. 2022). However, among these advancements, challenges persist in predicting the spatial distribution of soil erosion, including constraints related to time, cost, facilities, and result accuracy (KUCUKER, D.M. and GIRALDO, D.C. 2022). Recent years have witnessed the integration of remote sensing techniques and Geographic Information Systems (GIS), overcoming these limitations and enabling the prediction of soil erosion in larger areas with reasonable cost and accuracy (ASLAM, B. *et al.* 2021; ALAM, N.M. *et al.* 2022; ALIZADEH, M. *et al.* 2022; KUCUKER, D.M. and GIRALDO, D.C. 2022; HAYATZADEH, M. *et al.* 2023).

The investigated area, Kalat-e-Naderi county, located in a partially loess-covered region in northeast Iran, becomes the focal point of our study. Some areas of the county are dedicated to agriculture, while crop production is active on less steep slopes, emphasizing the need to address soil erosion, particularly in loess-covered regions, for sustainable food production. Loess is an eolian (windblown) pale yellow sediment (PYE, K. and TSOAR, H. 1987; FENN, K. *et al.* 2022), which besides its agricultural importance, serves as a crucial repository of Quaternary climate changes (XU, J. *et al.* 2022), offering a comprehensive terrestrial record of interglacial-glacial cycles. It stands out as a significant geological formation that captures the dynamic shifts in environmental conditions over time (MARKOVIČ, S.B. *et al.* 2014). Defined as sediment entrained, transported,

and deposited by the wind, and diagenetised *in situ*, loess is characterized by the predominance of silt-sized particles (WANG, X. *et al.* 2017), ranging from 2 μm to 50 μm in diameter (SMALLEY, I. *et al.* 2011). While most loess deposits exhibit a composition that includes measurable amounts of sand (> 50 μm) and clay (< 2 μm), the distinctive feature of loess lies in its prevalent content of silt-sized particles, typically ranging from 60 to 90 percent (MUHS, D.R. 2007). Due to its elevated porosity and silt content, loess is acknowledged as one of the most fertile forms of unconsolidated sedimentary rock. The inherent porosity of loess facilitates the absorption of gases containing carbon and nitrogen, enabling the provision of water and dissolved nutrients to plants through capillary rise during dry periods (RICHTHOFEN, F. 1872; EMERSON, W.W. and MCGARRY, D. 2003). However, the susceptibility of loess to erosion is evident, as it can be easily eroded by surface water, making it prone to the formation of subcutaneous hollow landforms (PÉCSI, M. 1990; WU, Q. *et al.* 2019). Consequently, the sensitivity of loess landforms to erosion highlights their significance in the context of natural hazards and related issues.

While numerous studies have delved into the well-known northern loess regions of Iran (e.g., Aqband, Neka, Maraveh Tappeh, etc.) (KHORMALI, F. *et al.* 2009; ASADI, S. *et al.* 2013; GHAFARPOUR, A. *et al.* 2016, 2023; GHARIBREZA, M. *et al.* 2020; SHARIFIGARM DAREH, J. *et al.* 2020) few investigations have specifically focused on the Kalat-e-Naderi loess region (OKHRAVI, R. and AMINI, A. 2001; KARIMI, A. *et al.* 2011), particularly in terms of erosion and with a geomorphological approach.

Against the backdrop of the unique characteristics and challenges posed by loess-covered areas, this study has two aims: 1) to generate soil erosion susceptibility maps in the less known, and less investigated loess-covered region of northeast Iran using the AHP method, and 2) to analyse the role of soil erosion in shaping various geomorphological landforms within the study area, employing a geomorphological approach.

Material and methods

Study area

The study area is located near the Iran-Turkmenistan border and is recognized as one of the loess-covered regions within the Khorasan-e-Razavi province. This region encompasses four basins including Archangan, Kalat, Qaratigan, and Chahchaheh basins, arranged from northwest to southeast (Figure 1). Loess regions in the study area share a common chronological relationship with the loesses in the Caspian Lowlands, despite a more than 500 km between the two areas (KARIMI, A. et al. 2011). In the Kalat-e-Naderi region, the loess occurs in a patchy distribution with a thickness of up to 12 metres ((KARIMI, A. et al. 2011), which is notably less than the thickness of loesses in the Caspian Lowlands in the northern part of Iran (FRECHEN, M. et al. 2009; KEHL,

M. et al. 2021; FEIZI, V. et al. 2023). As reported by KARIMI, A. et al. (2011), the sand, silt, clay, gypsum, and carbonate contents of Kalat-e-Naderi sections are 10–18, 67–86, 4–16, 11–25, and 2–12 percent, respectively, showing the typical loess characteristics (PÉCSI, M. 1990). Loess deposits are predominantly distributed on the north-eastern slopes of the Kopeh Dagh mountain range, covering a plateau-like geomorphic surface within a synclinal structure (KARIMI, A. et al. 2011).

The Kopeh Dagh mountain range demonstrates a northwest-southeast orientation. From a structural geological standpoint, the region showcases numerous folds, faults, and fissures, with the primary fault direction oriented northwest-southeast. The formation of synclines and anticlines in this area can be attributed to the predominant northwest-southeast directional pressure. According to the Digital Elevation Model (DEM) of the study area, the

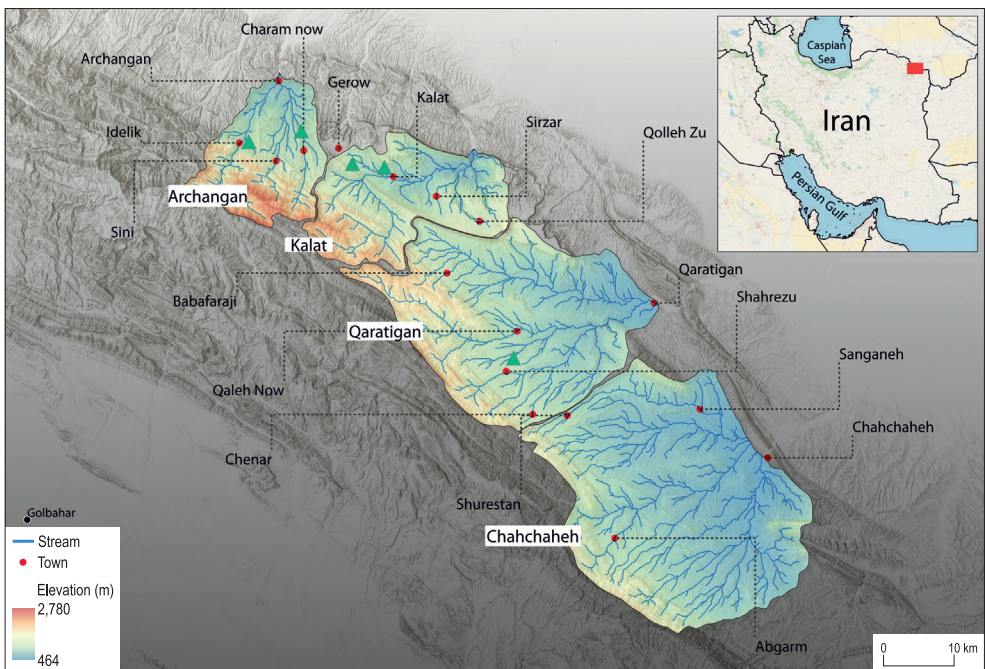


Fig. 1. The location of the studied basins in northeast Iran. The green rectangles indicate the positions of the visiting sites, as depicted in photos 1 through 5. Source: Authors' own elaboration.

highest and lowest elevations are recorded at 460 m and 2,780 m, respectively.

According to KÖPPEN's climate classification, Kalat-e-Naderi falls into the cold semi-arid (BSk) category (KÖPPEN, W. 1900). Climatic data from the Qaratigan watershed indicate a mean annual precipitation of 287 mm and a temperature of 12.2 °C (AMINI, A. 1995).

Historical climatic data for the area and its surroundings reveal significant seasonal variations in precipitation. The highest amounts (averaging 46.6 mm) occur between late January and the end of April, while the lowest precipitation values are observed between June and October (0.2 mm in August). Due to the arid and semi-arid climate, precipitation characteristics differ from more humid regions. In such arid and semi-arid regions, precipitation typically manifests as short but intense rainfall events (GHAHRAMAN, K. and NAGY, B. 2023).

Overall, in pursuit of our objectives, we employed the AHP methodology, coupled with remotely sensed data (e.g., digital elevation models and optical satellite imagery), GIS tools (e.g., ArcGIS and QGIS), and field surveys.

Analytic Hierarchy Process

The AHP is a suitable technique for identifying and mapping erosion-prone areas (BELKENDIL, A. et al. 2018; BELLOULA, M. et al. 2020; ASLAM, B. et al. 2021; SINSHAW, B.G. et al. 2021; EBHUOMA, O. et al. 2022). AHP is a method that compares qualitative factors and expresses them as numerical values. This research used AHP due to its advantages, such as the availability of input factors, the capability of comparing multiple parameters, and ease of use (RAJESH, C. et al. 2016; BELKENDIL, A. et al. 2018; TAIRI, A. et al. 2019). Table 1 shows the numerical scale (by SAATY, R.W. 1987) proposed to be used as a source for the pairwise comparison. Depending on the im-

Table 1. Pairwise comparison scale*

Rating scale	Numerical	Reciprocal
Extremely preferred	9	1/9
Very strongly to extremely preferred	8	1/8
Very strongly preferred	7	1/7
Strongly to very strongly preferred	6	1/6
Strongly preferred	5	1/5
Moderately to strongly preferred	4	1/4
Moderately preferred	3	1/3
Equally to moderately preferred	2	1/2
Equally preferred	1	1

*Proposed by SAATY, R.W. 1987.

portance of the selected factors, AHP assigns a value of 1 to 9 to each factor to decide the significance of the factor in association with the objective.

The AHP method comprises three primary steps. The initial step involves selecting the pertinent criteria for erosion. Criterion selection is contingent upon the impact of each factor on the occurrence of the phenomenon, our knowledge about the study area, insights gleaned from related researches, and crucially, the availability of data for each region (ARABAMERI, A. et al. 2018; AZAREH, A. et al. 2019; NEJI, N. et al. 2021; KUCUKER, D.M. and GIRALDO, D.C. 2022). Considering these critical considerations, we selected 7 factors including slope, aspect, elevation, drainage density, lithology, normalized difference vegetation index (NDVI), and precipitation. The flowchart and factors utilized in the AHP method for our study are depicted in Figure 2. Maps corresponding to each factor were generated using ArcMap and QGIS software (Figure 3).

One of the key geomorphological parameters influencing erosion is topography (RAHMATI, O. et al. 2016). Topographic factors, including slope, aspect, and elevation, were derived from the SRTM (1 Arc sec) Digital Elevation Model. The substantial influence of slope gradient on soil erosion is widely acknowledged (SAINI, S.S. et al. 2015; MESHAM, S.G. et al. 2022; OLI, M.R. et al. 2023). Hence, it is imperative to recognize slope as a pivotal factor in studies pertaining to soil erosion, given its profound impact on the phenomenon (ASLAM, B. et al. 2021).

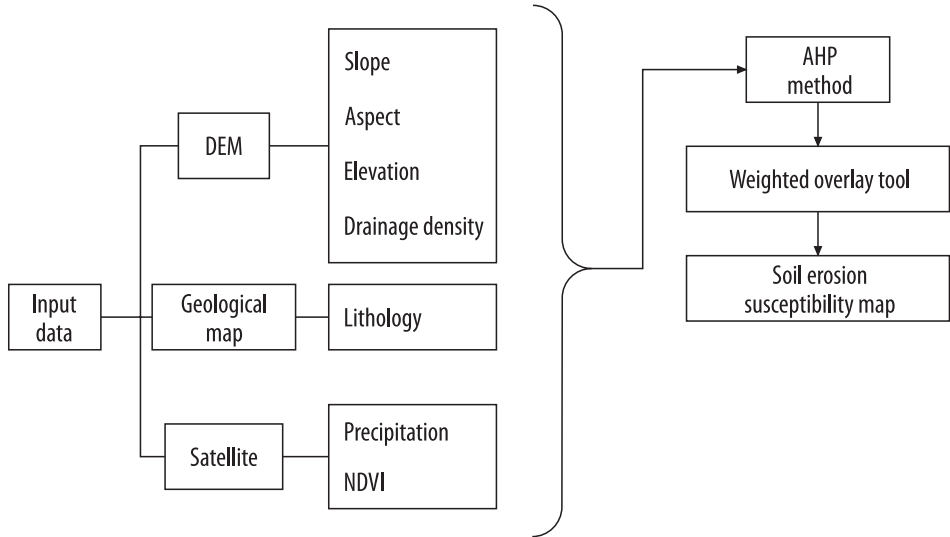


Fig. 2. The flowchart depicting the AHP method and the input data utilized for soil erosion susceptibility mapping. Source: Authors' own elaboration.

The slope map in our study was categorized into nine classes: 0° – 5° , 5° – 10° , 10° – 15° , 15° – 20° , 20° – 25° , 25° – 30° , 30° – 35° , 35° – 40° , and $> 40^{\circ}$ (see Figure 3, a). Considering the impracticality of agricultural expansion on steep slopes, the effective slope limit for erosion was set at 40° . Aspect influences erosion by regulating vegetation type, moisture, evaporation and transpiration, and sunlight exposure duration (JAAFARI, A. *et al.* 2014).

The aspect map encompasses ten directional classes: flat (-1°), north (0° – 22.5°), northeast (22.5° – 67.5°), east (67.5° – 112.5°), southeast (112.5° – 157.5°), south (157.5° – 202.5°), southwest (202.5° – 247.5°), west (247.5° – 292.5°), northwest (292.5° – 337.5°), and north (337.5° – 360°) (see Figure 3, b).

Elevation, by impacting vegetation type and precipitation, can affect erosion and gully development (GÓMEZ-GUTIÉRREZ, Á. *et al.* 2015). Given the mountainous nature of the area, this study adopted an eight-category elevation map with 290-metre elevation intervals to allow for more precise weight assignments for each category. The elevation categories include 460–750 m,

750–1,040 m, 1,040–1,330 m, 1,330–1,620 m, 1,620–1,910 m, 1,910–2,200 m, 2,200–2,490 m, and 2,490–2,780 m (see Figure 3, c).

The drainage density map, extracted from SRTM-DEM using the line density tool in ArcGIS 10.3, was divided into seven classes to construct the AHP comparison matrix with higher precision. The drainage density classes include 0.02–0.52, 0.52–1.02, 1.02–1.52, 1.52–2.02, 2.02–2.52, 2.52–3.02, and 3.02–3.70 (see Figure 3, d).

The lithology raster layer was prepared based on the 1:250,000 scale geologic map of the study area (see Figure 3, e). The study area, including 16 major lithological units, was divided into two categories, namely loess and solid rocks, given the focus on loess and erosion in loess-covered regions. It is important to note that the number of classes for factors such as slope, elevation, and drainage density may vary depending on the specific characteristics and conditions of each study area.

Numerous studies have highlighted the significance of precipitation and NDVI as influential factors in erosion susceptibility mapping using AHP (ALEXAKIS, D.D. *et al.*

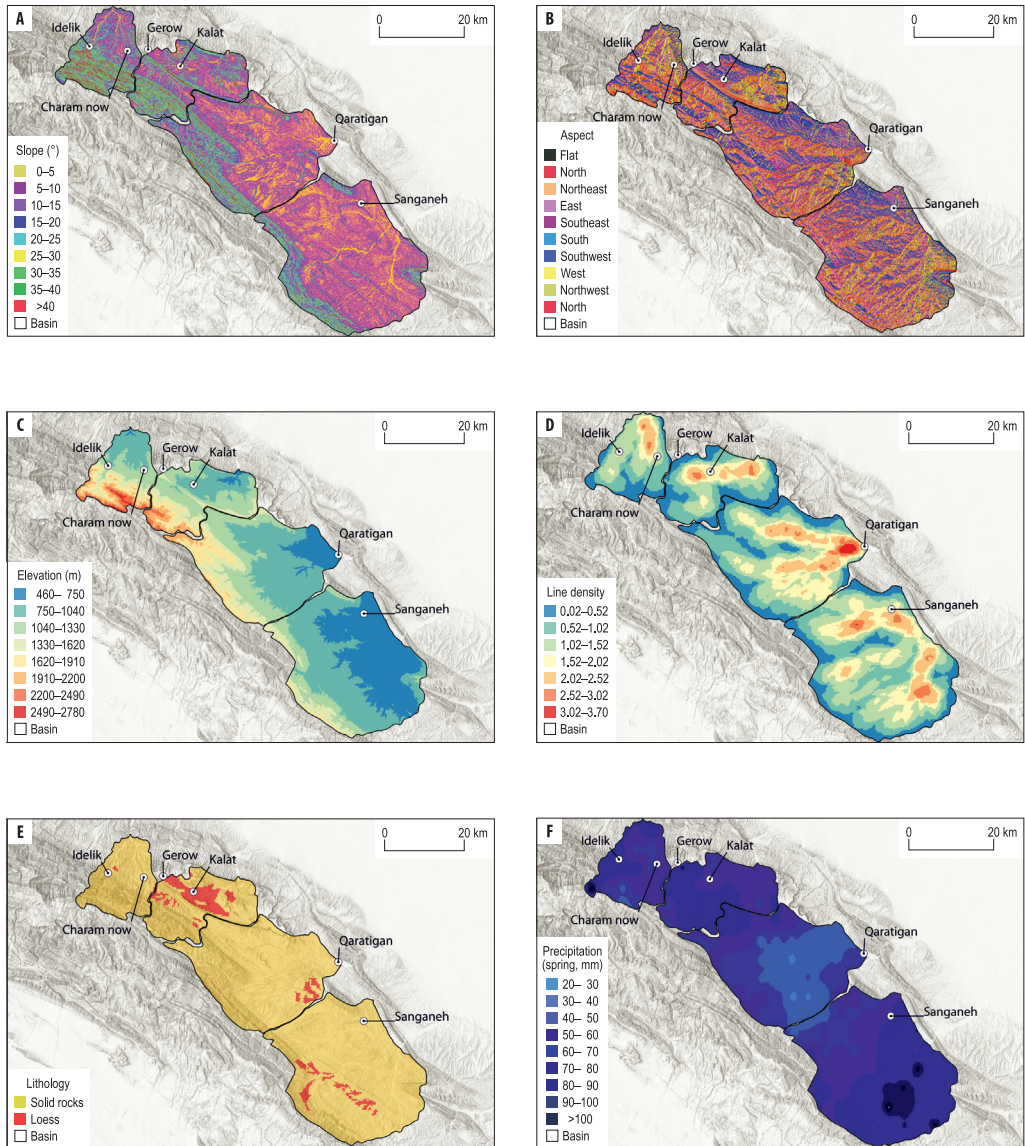


Fig. 3. Erosion contributing factor layers of the study area: slope (a), aspect (b), elevation (c), line density (d), lithology (e), and precipitation for spring (f). Source: Authors' own elaboration.

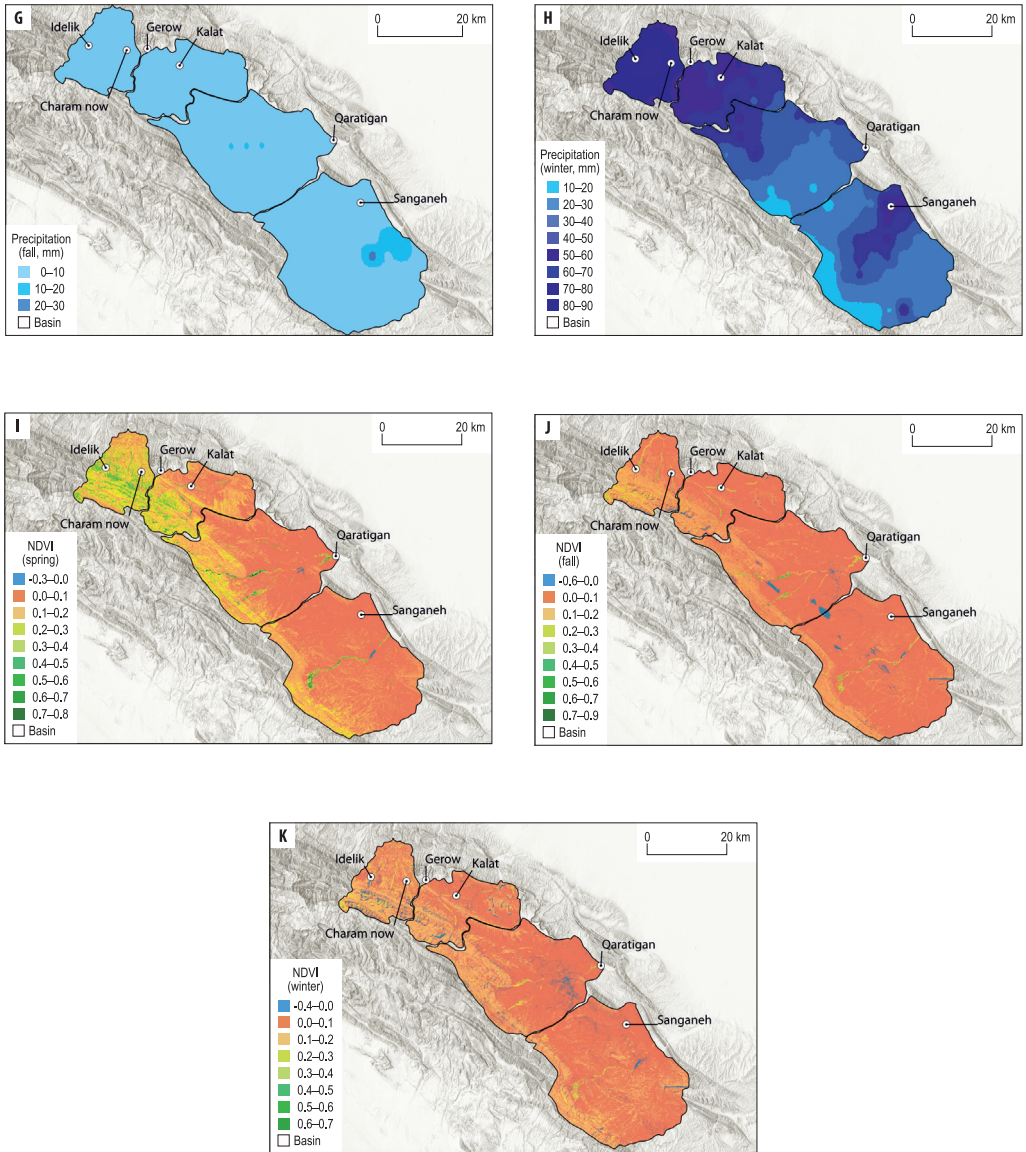


Fig. 3. Continued – Erosion contributing factor layers of the study area: precipitation for autumn, and winter (g, h), and NDVI for spring, autumn, and winter (i, j, k). Source: Authors' own elaboration.

2013; KACHOURI, S. et al. 2015; TAIRI, A. et al. 2019; ASLAM, B. et al. 2021; BOUAMRANE, A. et al. 2021; SANDEEP, P. et al. 2021; MUSHTAQ, F. et al. 2023). However, it has been observed that many researchers have relied on mean annual precipitation data (KACHOURI, S. et al. 2015; BOUFELDJA, S. et al. 2020; NEJI, N. et al. 2021), disregarding the uneven distribution of precipitation across different seasons. To overcome this limitation and improve the accuracy of the erosion susceptibility maps, it is essential to consider seasonal precipitation data. This is crucial because varying precipitation values have an impact on other factors and, more broadly, on erosional processes. By incorporating seasonal variability, our study can provide more accurate and nuanced insights into the spatiotemporal dynamics of soil erosion and inform more effective soil conservation strategies, particularly given the significance of agricultural activities in the study area.

In our study, we encountered the unavailability of meteorological station data for the study area. As a solution, we obtained precipitation data from the Center of Hydrometeorology and Remote Sensing (CHRS), University of California, Irvine, data portal (<https://chrsdata.eng.uci.edu>). To generate a comprehensive precipitation map for the year 2021, we utilized ArcMap and employed the Inverse Distance Weighted (IDW) interpolation method specifically for the spring, autumn, and winter seasons (see Figure 3, f, g, h). It is worth noting that since there was no recorded precipitation during the summer of 2021, the summer map depicting precipitation and NDVI was excluded from our analysis.

The NDVI maps were extracted from Sentinel-2 images using ArcMap. NDVI values range from -1 to +1 and are calculated using the following equation (FARAH, A. et al. 2021; PARSIAN, S. et al. 2021; DURLEVIĆ, U. et al. 2022):

$$NDVI = (NIR - RED) / (NIR + RED) \quad (1)$$

In Equation (1) *NIR* represents the near-infrared (band 8), and *RED* corresponds to the red band (band 4) of the Sentinel-2 im-

agery. *NDVI* values less than zero indicate the presence of water bodies and moisture, while values near zero (0–0.2) signify bare surfaces, rocks, sand, and snow. Values from 0.2 to 0.4 indicate areas covered by shrubs, grassland, and crops, while values exceeding 0.4 signify the presence of dense vegetation, such as orchards and, in certain regions, rice fields (see Figure 3, f, g, h).

The second step in the AHP involves assigning weights to the chosen criteria and conducting pairwise comparisons, a process that must also be extended to the sub-classes of each criterion. As presented in Table 1, each factor is assigned a value ranging from 1 to 9 based on its perceived importance or impact on erosion. The final step entails constructing a pairwise comparison matrix using the values assigned to the factors in the previous step. In AHP, the acceptable limit for the consistency ratio is equal to or less than 10 percent (SAATY, T.L. 1988; ALONSO, J.A. and LAMATA, M.T. 2006). The consistency ratio (*CR*) and consistency index (*CI*) are determined using the following equations:

$$CR = \frac{CI}{RI} \quad (2)$$

where *CI* is the consistency index, and *RI* is the random consistency index that is obtained from Table 2 (SAATY, T.L. and VARGAS, L.G. 2001). *CI* is calculated using the following equation:

$$CI = \frac{(\beta_{max} - n)}{n - 1} \quad (3)$$

where β_{max} is the largest eigenvalue of the comparison matrix, and *n* is the comparison matrix size. The process of determining the priority or weight for each factor involves calculating the eigenvalue (COSTA, C.A.B. and VANSNICK, J.-C. 2008). The eigenvalue is obtained by summing the products of each element in the eigenvector and the sum of the reciprocal matrix. To affirm the consistency of the given values, the consistency ratio (*CR*) must be calculated for each factor's pairwise comparison, as well as for the pairwise comparison of each factor's subclasses.

Table 2. Random consistency index (RI) values

n	RI	n	RI	n	RI
1	0.00	4	0.90	7	1.32
2	0.00	5	1.12	8	1.41
3	0.58	6	1.24	9	1.45

The erosion susceptibility maps for the study area were generated using the weighted overlay tool in ArcMap. The values assigned in the tool were selected based on the weight or importance of each class. Subsequently, the validation process was conducted through field surveys on visiting sites (see Figure 1). Field surveys allowed us to assess the model's success in identifying susceptible areas.

Results

As mentioned earlier, AHP pairwise comparison was drawn during the AHP preparation stages. Subsequently, the pairwise comparison tables and erosion susceptibility maps for each season are presented.

The spring season

In pairwise comparison, a score of 1 indicates equal importance, while a score of 9 signifies very high importance of one factor over the other (Саагу, Т.Л. 1980) (see Table 1). The pairwise comparison table for the spring season (Table 3) reveals that precipitation, lithology, slope, and drainage density carry the highest weights among the factors, with values of 0.34, 0.22, 0.13, and 0.10, respectively.

Conversely, elevation (0.06), aspect (0.07), and NDVI (0.08) have the least impact on erosion in the spring season.

Slope, with a score value of 3, is moderately preferred over aspect and elevation. Over 716 km² of the area falls within slope categories between 15° and 40°. Field observations highlighted that these slopes, due to the presence of soil and agricultural development, are particularly prone to erosion. Consequently, a value of 8 is assigned to these sub-criteria in the weighted overlay tool. Lithology is moderately preferred over all factors except precipitation. Field observations confirmed various forms of erosion on loess-covered surfaces, indicating that loess is highly susceptible to erosion even with minimal rainfall. Thus, loess is assigned a value of 8 as a sub-criterion of lithology. In the spring season, precipitation is moderately to strongly preferred over aspect, NDVI, and drainage density (see Table 3). The highest precipitation values in the spring season (90–100 mm, and >100 mm) receive a score value of 9 in the weighted overlay tool, indicating the highest importance in erosion. To validate the assigned values, the consistency ratio was computed, yielding a spring season consistency ratio of 0.06, affirming the correct assignment of weights to the factors.

The autumn season

According to Table 4, precipitation (0.26), lithology (0.23), and slope (0.14) emerge as the most influential factors contributing to erosion in the autumn season. Conversely, NDVI

Table 3. Pairwise comparison table of the spring season

Pairwise comparison	Slope	Aspect	Lithology	Elevation	NDVI	Precipitation	Drainage density	Weight
Slope	1	3	1/3	3	1	1/3	2	0.13
Aspect	1/3	1	1/3	1	2	1/4	1/2	0.07
Lithology	3	3	1	3	3	1/3	3	0.22
Elevation	1/3	1	1/3	1	1/2	1/3	1/2	0.06
NDVI	1	1/2	1/3	2	1	1/4	1/2	0.08
Precipitation	3	4	3	3	4	1	4	0.34
Drainage density	1/2	2	1/3	2	2	1/4	1	0.10

CR: 0.06

Table 4. Pairwise comparison table of the autumn season

Pairwise comparison	Slope	Aspect	Lithology	Elevation	NDVI	Precipitation	Drainage density	Weight
Slope	1	1/2	1/2	2	2	1/2	3	0.14
Aspect	2	1	1/3	1	2	1/3	1	0.12
Lithology	2	3	1	3	3	1/2	3	0.23
Elevation	1/2	1	1/3	1	2	1/2	2	0.10
NDVI	1/2	1/2	1/3	1/2	1	1/3	1	0.07
Precipitation	2	3	2	2	3	1	2	0.26
Drainage density	1/3	1	1/3	1/2	1	1/2	1	0.08

CR: 0.05

and drainage density, with weight values of 0.07 and 0.08, respectively, exhibit the least influence on erosion during the autumn season. Aspect and elevation, carrying weight values of 0.12 and 0.10, prove to be more impactful than NDVI and drainage density, yet less significant than precipitation, lithology, and slope. In terms of preference, lithology and precipitation are moderately favoured over aspect and NDVI. Notably, slope, with a score value of 3, is moderately preferred in comparison to drainage density. Given the semi-arid climate of Kalat-e-Naderi region, the erosion in the region can be influenced even by minimal rainfall. The primary agents of erosion during the autumn season are the areas covered by loess, coupled with precipitation and steep slopes. The consistency ratio for the autumn season (0.05) assures the reliability of the assigned weights.

The winter season

Precipitation, lithology, slope, and drainage density emerge as the most impactful factors on erosion during the winter season, with respective weight values of 0.33, 0.23, 0.14, and 0.10 (Table 5). Elevation, aspect, and NDVI carry lower weights of 0.07, 0.07, and 0.06, indicating their relatively lesser influence on erosion. Precipitation, with score values of 3 and 4, is moderately to strongly preferred over aspect and NDVI, and moderately preferred over slope, lithology, elevation, and drainage density. As depicted previously, the Archangan and Kalat basins receive the highest amount of precipitation during the winter season (see Figure 3, h),

while the spring season precipitation is distributed almost evenly across the four basins (see Figure 3, f), with Archangan, Kalat, and Chahchaheh being more prominent. For the weighted overlay tool, the assigned value for the highest amount of precipitation (80–90 mm) is 8 (Table 6). Furthermore, lithology, scoring 3, is moderately preferred over slope, aspect, elevation, NDVI, and drainage density. Recognizing the susceptibility of loess to erosion, it is assigned a value of 8 in the weighted overlay tool (see Table 6). The winter season's consistency ratio of 0.04 falls within an acceptable range, affirming the reliability of the assigned weights.

The calculated consistency ratio for each factor's sub-classes, as presented in Table 6, is below 10 percent (< 0.1), meeting the acceptable threshold. Subsequently, erosion susceptibility maps were generated in ArcGIS 10.3 using the weighted overlay tool. Values ranging from 1 to 9 were assigned in the tool based on the weight assigned to each subclass. The Weighted Overlay Tool operates according to Equation (4) (FEIZIZADEH, B. et al. 2014; ARABAMERI, A. et al. 2018; KAHSAI, A. et al. 2018; TAIRI, A. et al. 2019; BOUFELDJA, S. et al. 2020; ASLAM, B. et al. 2021), wherein the dataset is multiplied by its weight, and the sum of all results yields the erosion susceptibility (ES) value for each pixel.

$$ES = [(Sl \cdot W) + (As \cdot W) + (Li \cdot W) + (El \cdot W) + (NDVI \cdot W) + (Pr \cdot W) + (Drd \cdot W)], \quad (4)$$

where Sl is the slope, As is the aspect, Li is the lithology, El is the elevation, Pr is the precipitation, Drd is the drainage density, and W

Table 5. Pairwise comparison table of the winter season

Pairwise comparison	Slope	Aspect	Lithology	Elevation	NDVI	Precipitation	Drainage density	Weight
Slope	1	3	1/3	3	2	1/3	2	0.14
Aspect	1/3	1	1/3	1	2	1/4	1/2	0.07
Lithology	3	3	1	3	3	1/3	3	0.23
Elevation	1/3	1	1/3	1	1	1/3	1/2	0.07
NDVI	1/2	1/2	1/3	1	1	1/4	1/2	0.06
Precipitation	3	4	3	3	4	1	3	0.33
Drainage density	1/2	2	1/3	2	2	1/3	1	0.10

CR: 0.04

Table 6. Weight, consistency ratio (CR), and assigned values to the weighted overlay tool of all sub-classes of each factor

Criteria	CR	Sub-criteria	Weights	Assigned values to weighted overlay tool
Slope	0.007	0–5°	0.020	1
		5–10°	0.031	2
		10–15°	0.044	3
		15–20°	0.177	8
		20–25°	0.177	8
		25–30°	0.177	8
		30–35°	0.177	8
		35–40°	0.177	8
>40°	0.020	1		
Aspect	0.030	Flat	0.021	1
		North	0.074	5
		Northeast	0.074	5
		East	0.035	2
		Southeast	0.222	7
		South	0.222	7
		Southwest	0.222	7
		West	0.035	2
Northwest	0.095	5		
Lithology	0.000	Solid rocks	0.111	4
		Loess	0.889	8
Elevation	0.006	460–750	0.030	1
		750–1,040	0.135	5
		1,040–1,330	0.135	5
		1,330–1,620	0.135	5
		1,620–1,910	0.231	6
		1,910–2,200	0.231	6
		2,200–2,490	0.051	2
		2,490–2,780	0.051	2
Drainage density	0.010	0.02–0.52	0.041	1
		0.52–1.02	0.061	2
		1.02–1.52	0.101	3
		1.52–2.02	0.113	3
		2.02–2.52	0.169	4
		2.52–3.02	0.258	5
		3.02–3.70	0.258	5

Table 6. Continued

Criteria	CR	Sub-criteria	Weights	Assigned values to weighted overlay tool
NDVI (spring)	0.003	-0.31–0.0	0.043	1
		0.0–0.1	0.223	4
		0.1–0.2	0.223	4
		0.2–0.3	0.137	3
		0.3–0.4	0.075	2
		0.4–0.5	0.075	2
		0.5–0.6	0.075	2
		0.6–0.7	0.075	2
NDVI (autumn)	0.006	0.7–0.83	0.075	2
		-0.56–0.0	0.075	1
		0.0–0.1	0.140	2
		0.1–0.2	0.140	2
		0.2–0.3	0.271	3
		0.3–0.4	0.075	1
		0.4–0.5	0.075	1
		0.5–0.6	0.075	1
NDVI (winter)	0.004	0.6–0.7	0.075	1
		0.7–0.86	0.075	1
		-0.37–0.0	0.047	1
		0.0–0.1	0.241	4
		0.1–0.2	0.241	4
		0.2–0.3	0.146	3
		0.3–0.4	0.081	2
		0.4–0.5	0.081	2
Precipitation (spring)	0.090	0.5–0.6	0.081	2
		0.6–0.7	0.081	2
		20–30	0.015	2
		30–40	0.021	3
		40–50	0.031	4
		50–60	0.047	5
		60–70	0.071	6
		70–80	0.107	7
Precipitation (autumn)	0.000	80–90	0.162	8
		90–100	0.239	9
		>100	0.307	9
Precipitation (winter)	0.030	0–10	0.250	1
		10–20	0.250	1
		20–30	0.500	2
		10–20	0.024	1
		20–30	0.033	2
		30–40	0.048	3
		40–50	0.071	4
50–60	0.106	5		
60–70	0.157	6		
70–80	0.231	7		
80–90	0.331	8		

represents the weight value of each factor. In this study, Equation 4 is applied three times as each factor's weight has three different values associated with three distinct seasons.

Figures 4, 5, and 6 depict the final erosion susceptibility maps for each season. Employing the natural break method (SHAHABI, H. and HASHIM, M. 2015; SAHA, S. et al. 2019), the maps

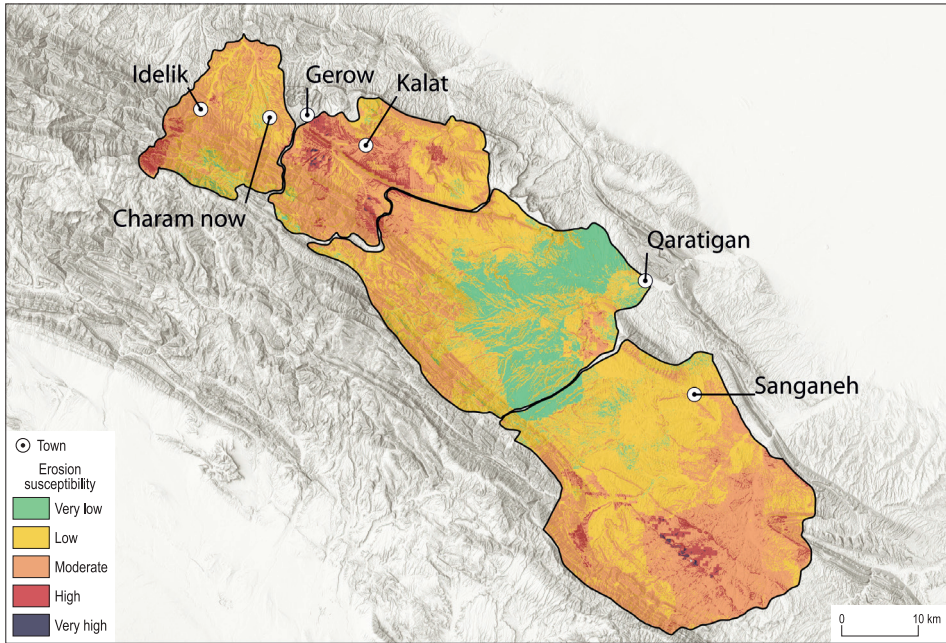


Fig. 4. AHP-based erosion susceptibility map of the spring season. *Source:* Authors' own elaboration.

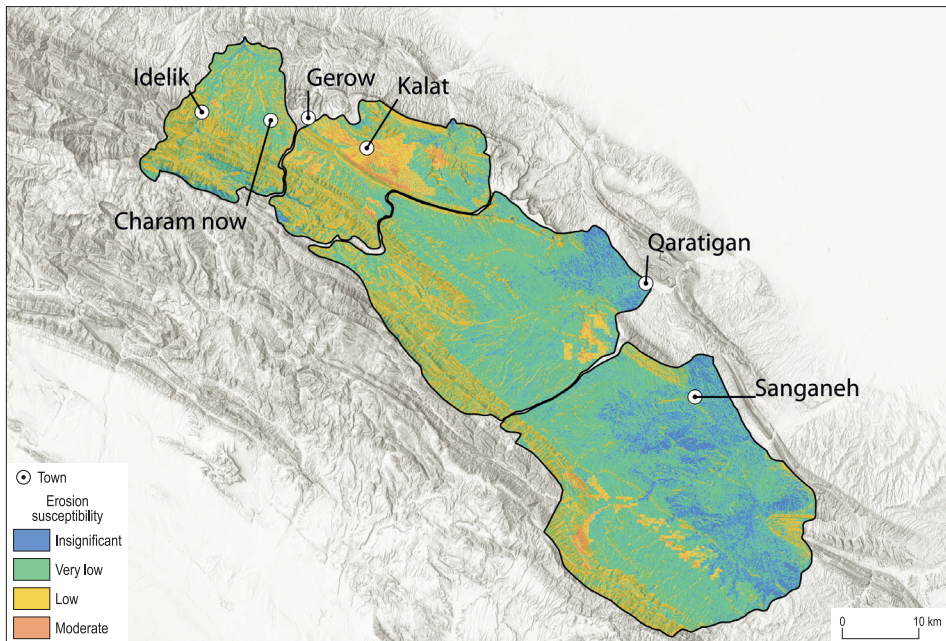


Fig. 5. AHP-based erosion susceptibility map of the autumn season. *Source:* Authors' own elaboration.

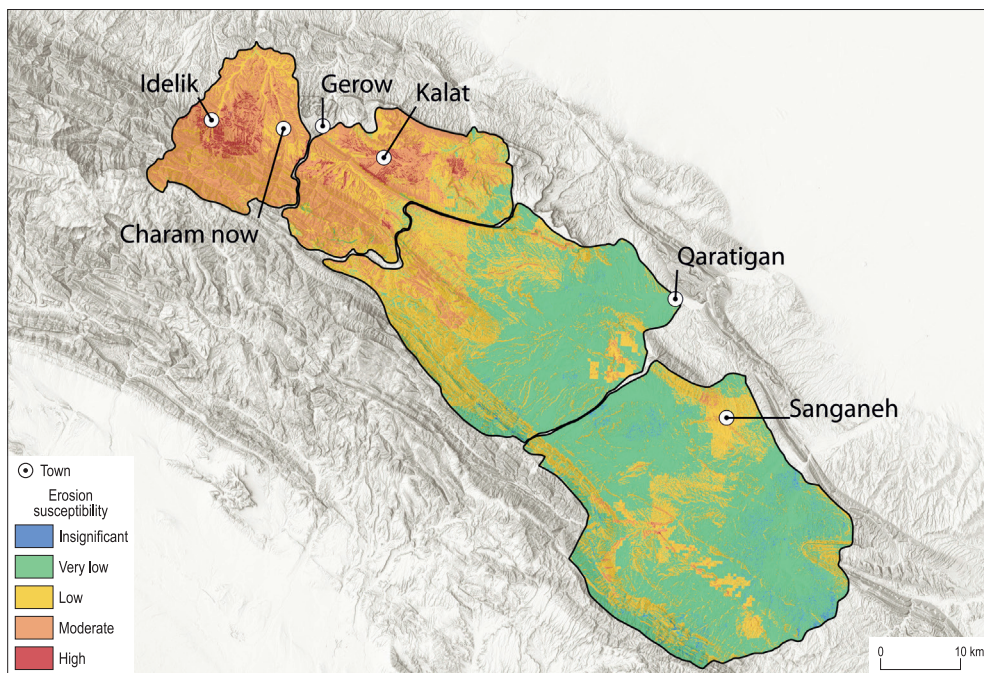


Fig. 6. AHP-based erosion susceptibility map of the winter season. *Source:* Authors' own elaboration.

were reclassified into six categories: insignificant, very low, low, moderate, high, and very high (EBHUOMA, O. et al. 2022). It is noteworthy that, owing to the seasonal variation in the impact of each factor, the erosion susceptibility maps encompass different categories.

The very high susceptibility class in the spring map (see *Figure 4*) is predominantly distributed in Chahchaheh and Kalat basins, covering an area of 2.511 km² in the study area. In contrast, the areas with very low erosion levels (259.59 km²) are mainly located in the central and north-eastern parts of the Qaratigan basin. The distribution of each erosion susceptibility class in the spring season is detailed in *Table 6*. The low (1,023.09 km²), and moderate (869.37 km²) erosion susceptibility classes cover the majority of the studied basins in the spring season. High erosion susceptibility areas are minor in the Qaratigan basin during the spring season. In Kalat and Chahchaheh basins, the high erosion susceptibility area

is primarily in the central section, while in the Archangan basin, the south-western part is mainly in the high erosion susceptibility class. Overall, 105.615 km² of the study area is classified as having high erosion susceptibility in the spring season.

The spring season erosion susceptibility map highlights that regions with the highest susceptibility to erosion are mainly associated with high precipitation values, loess cover, and steep slopes. Conversely, regions with the lowest susceptibility to erosion correspond to gentle slopes and lower precipitation values.

The winter season's erosion susceptibility map (see *Figure 6*) was categorized into five classes, ranging from insignificant to a high level. The Chahchaheh and Qaratigan basins are primarily covered with the very low (1,077.80 km²) and low (743.38 km²) classes, while the other two basins (Kalat and Archangan) are dominated by moderate (382.28 km²) and high (36.73 km²) classes (see *Table 7*). As shown in *Figure 6*, the areas

Table 7. Area and percentage of each class of erosion

Season	Insignificant		Very low		Low		Moderate		High		Very high	
	km ²	%	km ²	%	km ²	%	km ²	%	km ²	%	km ²	%
Spring	–	259.59	259.59	11.48	1,023.09	45.27	869.37	38.47	105.61	4.67	2.51	0.11
Autumn	12.00	1,370.45	1,370.45	60.65	591.79	26.19	26.29	1.16	–	–	–	–
Winter	0.88	1,077.80	1,077.80	47.69	743.38	32.90	382.28	16.91	36.73	1.62	–	–

with moderate and high erosion potential in winter coincide with the region covered by loess, which is very sensitive to water erosion. Thus, precipitation and lithology can be considered as the most dominant factors in the overall erosion process.

Discussion

Based on the pairwise comparisons (see *Tables 3, 4, and 5*), erosion has been more significantly influenced by precipitation and lithology than any other factors, as they consistently exhibit higher weights in all three pairwise comparison tables for each studied season. The increased impact of precipitation and lithology can be attributed to the relatively intense yet short downpours in the study area, leading to flash floods, rill and sheet erosion, especially on unresistant and unvegetated surfaces such as loess. GHAHRAMAN, K. and NAGY, B. (2023) have also reported intense rainfall in short time periods in arid and semi-arid regions of northeast Iran.

Field observations indicated that both active and inactive agricultural lands have been undergoing erosion (*Photo 1, a, b*). This observation aligns with our soil erosion maps, where high-susceptibility areas correspond to the location of agricultural lands. The increased vulnerability of agricultural lands to erosion can be attributed to their location on loess deposits, as well as human activities like cultivation and plowing, making the surface more prone to erosion (BENISTON, J.W. et al. 2015; ZHANG, J. et al. 2019).

According to the erosion susceptibility maps, the region around Gerow village falls into the high erosion susceptibility category in winter and spring seasons, and the

moderate category in the autumn season (see *Figures 4, 5, and 6*). Field observations confirm the presence of significant erosional features near Gerow village, including loess sinkholes, gully erosion, and suffusion (*Photo 1, a, d, and e*). The occurrence of sinkholes, even in agricultural lands, can be primarily attributed to the presence of water, especially in the form of precipitation, and lithology. In loess-covered regions, subsurface cracks allow rainfall to penetrate, extending existing fissures and washing away material, leading to the formation of sinkholes, gullies, and suffusion. It is noteworthy that field observations indicate the presence of small and occasionally large pebbles in the loess around Gerow. The existence of these materials in the loess suggests that, in this area, sediment/material transportation is not solely occurring through wind processes; water transportation has also been active in these areas.

In other areas classified as moderately to highly erosion-susceptible, such as the mountain slopes upstream of the abandoned agricultural lands near Gerow village, erosion has led to the exposure of bedrock (*Photo 1, c*). The presence of exposed bedrock highlights the significance of erosion in the study area. Large-scale erosional processes, including landslides, were also observed during field surveys (not in loess-covered sections) (*Photo 1, b*), underscoring the importance of mass movements in the area. Authorities and planners need to take these factors into consideration when planning in these areas.

Another visited site was Idelik village (see *Figure 1*), also classified in high and moderate erosion-susceptible classes on our maps. The predominant form of erosion in this area is the selective erosion of the folded structure

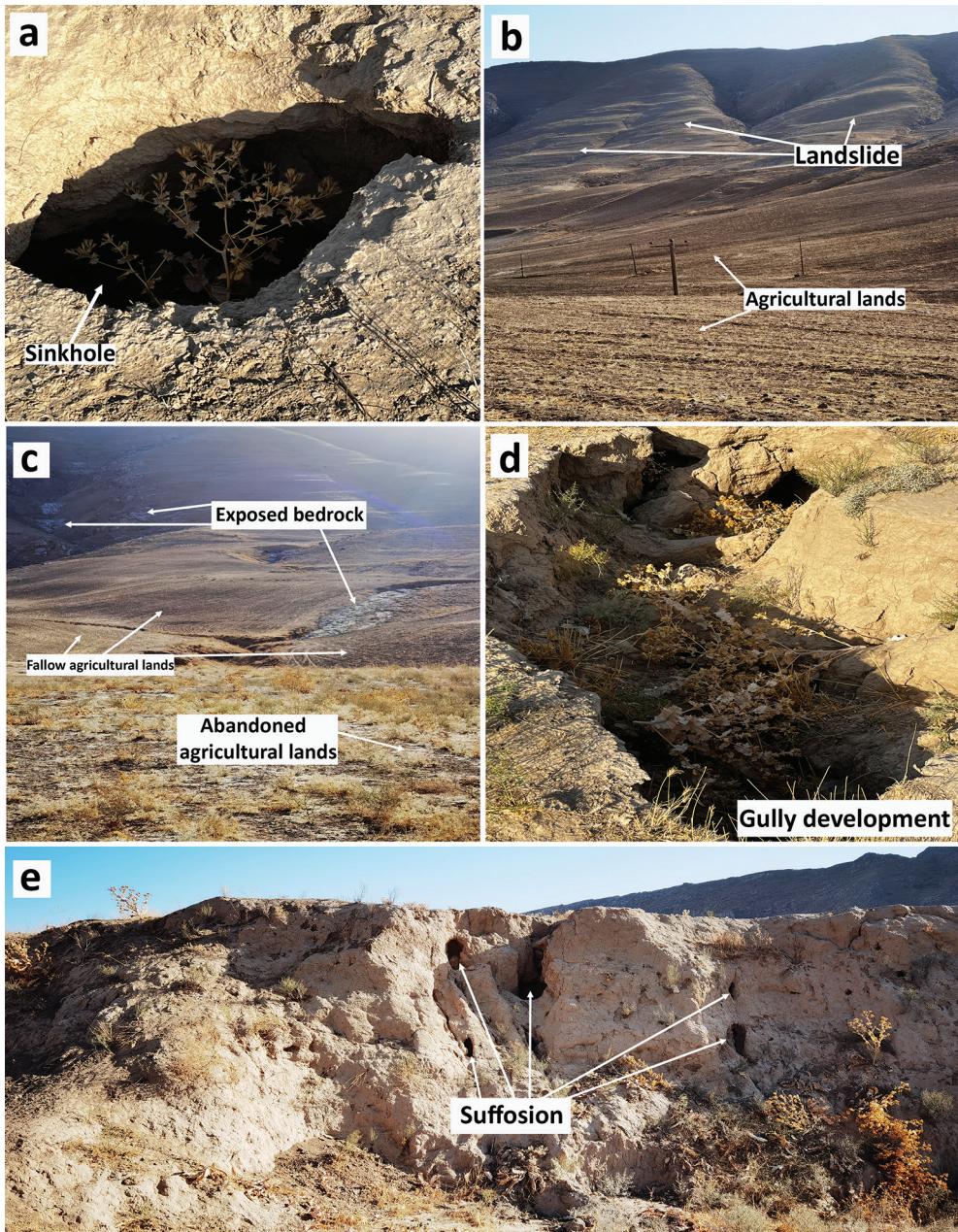


Photo 1. Validation sites around Gerow village. Sinkhole in an abandoned agricultural land (a), landslides in the vicinity of active agricultural fields (b), exposed bedrock on the slopes and in fallow agricultural fields (c), gully development on the abandoned agricultural fields (d), and suffusion on loess walls caused by CaCO_3 dissolution (e). Photos taken by the authors.

of the mountains by water and mass movements, resulting in steep walls from the more resistant layers and less steep slopes on the less resistant layers (*Photo 2, a*). Although this type of erosion does not directly impact farmlands in the study area, it holds significance from a hazard perspective. Our field observations revealed gully erosion, as well as topples and slides, especially around the

rice fields located on loess-covered lands (*Photo 2, b*). Additional erosional processes, such as solifluction and landslides, were observed on the slopes, exposing the underlying materials by removing the topsoil. This type of erosion resembles a minor mass movement, evident on the slopes.

According to our maps, the regions around the “Charam now” village are classified as

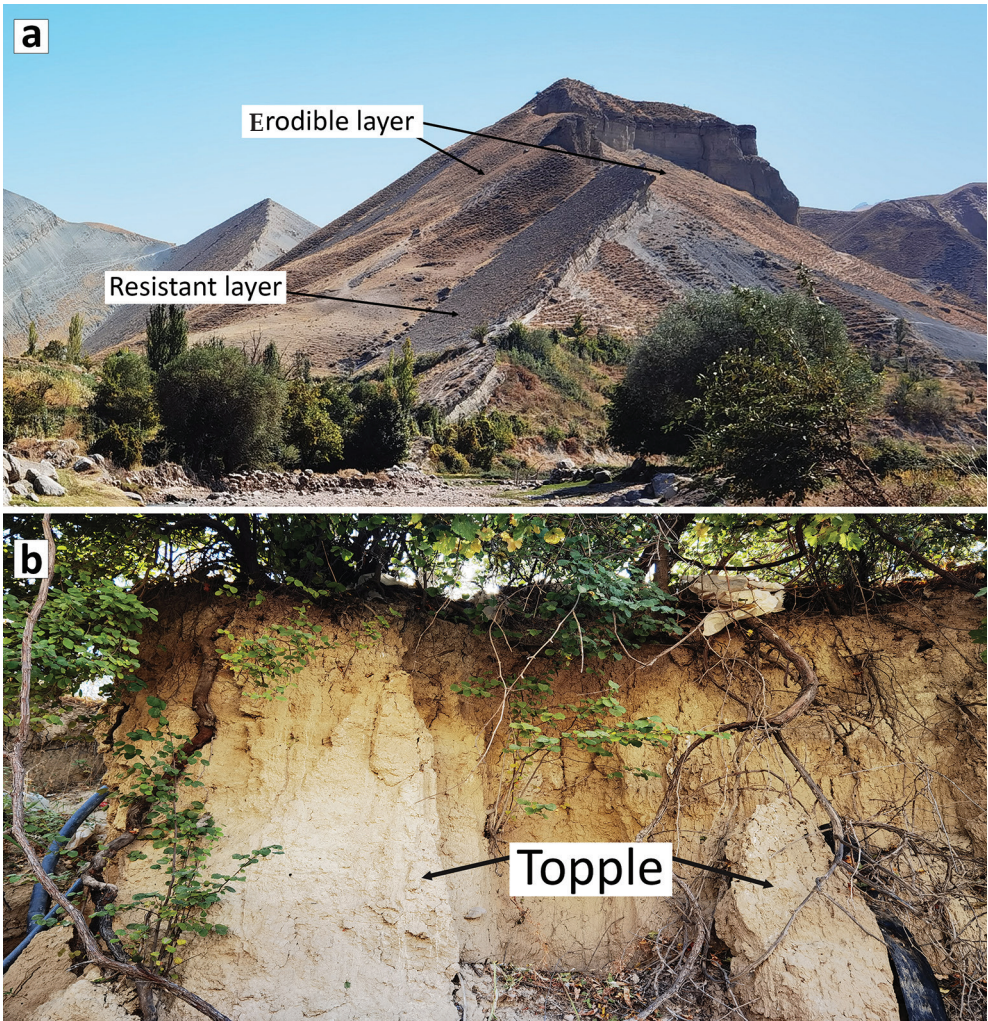


Photo 2. Validation sites around the Idelik village showing erodible layers on the erosion resistant underlying layer on the slopes (a), and columnar blocks being detached from the loess mass (topples) on the loess walls (b). Photos taken by the authors.

very low and low classes, while field observations reveal substantial soil erosion in this area. This discrepancy can be primarily attributed to the scale of the lithological map, as some parts of this area were not classified as loess. However, field observations showed strong erosion on the loess near this village. According to the lithological input, the model considered the lithology as resistant, classifying this area in very low and low soil erosion susceptible classes. It is noteworthy that we have systematically checked the entire basins for this issue, and the “Charam now” village and its surrounding area were the only instances where the lithological map did not accurately indicate the units. In general, fallen loess walls, gully development, fallen riverbanks, and small-scale landslides were observed in this area.

To examine remote or inaccessible areas of the “Charam now” village, we utilized Google Earth satellite imagery. Erosional features such as landslides and gullies near the village are illustrated in *Photo 3*. Local roads have been constructed to facilitate access to agricultural lands situated on the top of the hills. Instability of the slopes and increased chance of landslides in this area can also be related to anthropogenic activities such as road construction.

The majority of agricultural lands in the Kalat basin are located on slopes, with some fields occupying less inclined gradients. Ploughing these agricultural fields, in conjunction with the loess composition of the land and steeper slopes, has exacerbated erosion in this region, as evidenced by our soil erosion maps. With respect to cultivation, erosional processes in these loess-covered areas have the potential to adversely impact crop production. HARRIS, H.L. and DREW, W.B. (1943) have demonstrated that uneroded loess fields provide an environment that is 50–100 percent more favourable for plant growth than eroded loess fields. Observations of gully and sheet erosion, subsurface erosional features, and landslides in the Kalat basin indicate the prevalence of strong erosional processes in this area (*Photo 4*).

Considering the inherent limitations of the availability of relevant lithological map, namely its 1:250,000 scale and lack of detailed information and given our research focus on loess-covered regions, we opted to categorize the lithological map into two classes: loess and solid rocks. Solid rocks encompass both erodible and resistant rocks, such as limestone, shale, sandstone, and marl. Consequently, in the weighted overlay tool, loess was assigned a score of 8 due to its erosivity and prevalence in the study area, while solid rocks were assigned a score of 4, reflecting their lower susceptibility to erosion owing to the presence of resistant rocks (~ 740 km²). This approach aligns with other studies that have employed different weights for resistant and erodible rocks in their AHP models (ARABAMERI, A. *et al.* 2018; EL JAZOULI, A. *et al.* 2019; BOZALI, N. 2020).

In addition to precipitation and lithology, the influence of slope on soil erosion is significant. This is primarily attributed to the impact of slope on flow accumulation, runoff velocity, and surface instability (RAHMATI, O. *et al.* 2017). Multiple studies have demonstrated that even gentle slopes can be vulnerable to erosion and gully development (LE ROUX, J.J. and SUMNER, P. 2012; LUKIĆ, T. *et al.* 2018; ARABAMERI, A. *et al.* 2019; PHINZI, K. *et al.* 2021).

Vegetation cover in the study area has been subjected to overgrazing by livestock, such as goats and sheep, which can exacerbate soil erosion by removing protective vegetation cover. However, in our study area, we observed that animal footpaths have created micro-terrace structures on the slopes, while other slopes have remained intact from this process (*Photo 5*). This observation is consistent with the findings of AFRAH, H. *et al.* (2010), who reported that micro-terraces in the Golestan Province loesses have remained unchanged in terms of morphological structure for an extended period. This preservation is primarily attributed to the fact that animals have consistently used the old paths for grazing, leaving the vegetation cover intact in other parts of the rangeland.



Photo 3. The Google Earth image showing erosional features such as gullies and landslides as well as anthropogenic features such as agricultural lands and a road in the vicinity of the “Charam now” village. Authors’ own elaboration based on the Google Earth image.

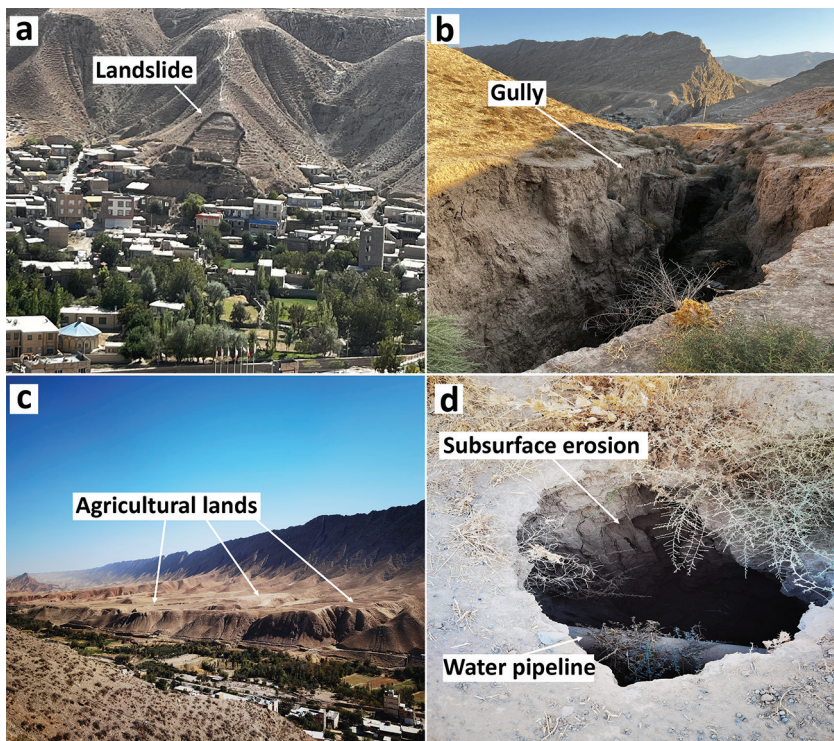


Photo 4. Validation sites in the vicinity of the Kalat city showing landslide (a), deep gully erosion (b), agricultural lands developed on loess-covered areas (c), and sinkholes created by the subsurface erosion on loess-covered areas impacting urban infrastructure (d). Photos taken by the authors.

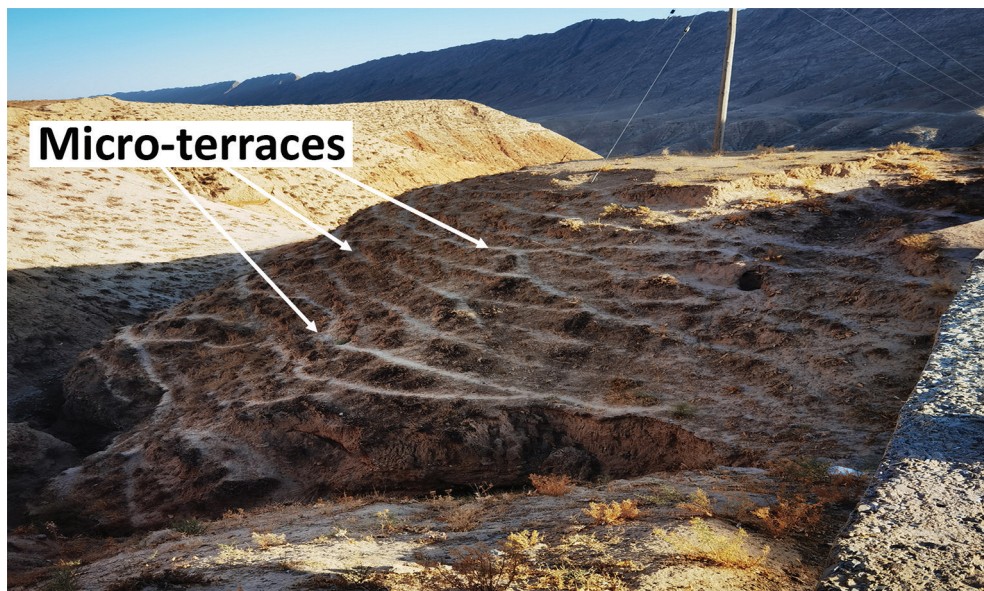


Photo 5. Micro-terraces created by livestock on the slopes of the study area.
Photo taken by NOOSHIN NOKHANDAN, F.

Conclusions

This research comprehensively investigated erosion-susceptible areas within the major basins of Kalat-e-Naderi county, situated in northeast Iran. The study's focal point was the dual nature of loess, serving as fertile ground for agriculture while presenting vulnerability to erosion. Leveraging the AHP method with 7 key parameters, including slope, aspect, elevation, lithology, NDVI, drainage density, and precipitation, we successfully delineated the spatial distribution of erosion-susceptible regions. The integration of seasonal data, accounting for variations in precipitation and vegetation cover, allowed for the creation of detailed erosion susceptibility maps. Key factors influencing water erosion, as identified through pairwise comparison tables, include precipitation, lithology, and slope. These findings have been visually represented on erosion susceptibility maps, highlighting areas prone

to erosion during different seasons. Notably, these vulnerable regions exhibit a discernible correlation with the three primary factors – precipitation, lithology, and slope – while the convergence of the additional four factors amplifies erosion.

Given the semi-arid climate of the region and the loess's heightened erodibility in wet seasons with higher precipitation, the research focused specifically on water erosion. Validation through field observations affirmed the accuracy of the erosion susceptibility maps where erosion-susceptible areas in the map correspond to the observed areas in the field. Despite limitations, such as the absence of comparable studies in neighbouring areas for validation, challenges in reaching erosion sites, and data constraints, the results of this method are invaluable. They offer actionable insights for policymakers and planners, facilitating effective damage mitigation and the formulation of preventative strategies.

Acknowledgements: We express our gratitude to the Stipendium Hungaricom program for their support. Additionally, we extend our thanks to the Erasmus + 20% project (2021-1-HU01-KA131-HED-000003804) for their financial assistance towards our fieldwork expenses. We would also like to acknowledge Professor Farhad KHORMALI for his invaluable scientific support and his dedication in facilitating our field observations. We also would like to thank the reviewers for their comments, which improved the quality of our work.

REFERENCES

- ABBAS, S., DASTGEER, G., YASEEN, M. and LATIF, Y. 2022. Land-use change impacts on soil and vegetation attributes in the Kanshi River basin, Potohar Plateau, Pakistan. *Land Degradation & Development* 33. (15): 2649–2662. Available at <https://doi.org/10.1002/ldr.4252>
- AFRAH, H., BARANI, H., BAHREMAND, A. and SHEIKH, V. 2010. Comparison of soil physical properties in micro terraces and inters micro terraces on rangelands. Case study: Baba Shamlak Ranch. *WJournal of Water and Soil Conservation* 17. (2): 141–153.
- AHMADI, M., MINAEI, M., EBRAHIMI, O. and NIKSERESHT, M. 2020. Evaluation of WEPP and EPM for improved predictions of soil erosion in mountainous watersheds: A case study of Kangir River basin, Iran. *Modelling Earth Systems and Environment* 6. (4): 2303–2315. Available at <https://doi.org/10.1007/s40808-020-00814-w>
- ALAM, N.M., JANA, C., MANDAL, D., MEENA, S.K., SHRIMALI, S.S., MANDAL, U., MITRA, S. and KAR, G. 2022. Applying Analytic Hierarchy Process for identifying best management practices in erosion risk areas of northwestern Himalayas. *Land* 11. (6): 1–18.
- ALEKSOVA, B., LUKIĆ, T., MILEVSKI, I., SPALEVIĆ, V. and MARKOVIĆ, S.B. 2023. Modelling water erosion and mass movements (Wet) by using GIS-based multi-hazard susceptibility assessment approaches: A case study – Kratovska Reka catchment (North Macedonia). *Atmosphere* 14. (7): 1–28.
- ALEXAKIS, D.D., HADJIMITSIS, D.G. and AGAPIOU, A. 2013. Integrated use of remote sensing, GIS and precipitation data for the assessment of soil erosion rate in the catchment area of “Yialias” in Cyprus. *Atmospheric Research* 131. 108–124. Available at <https://doi.org/10.1016/j.atmosres.2013.02.013>
- ALIZADEH, M., ZABIHI, H., WOLF, I.D., LANGAT, P.K., POUR, A.B. and AHMAD, A. 2022. Remote sensing technique and ICONA based-GIS mapping for assessing the risk of soil erosion: A case of the Rudbar Basin, Iran. *Environmental Earth Sciences* 81. (21): 512. Available at <https://doi.org/10.1007/s12665-022-10634-z>
- ALONSO, J.A. and LAMATA, M.T. 2006. Consistency in the analytic hierarchy process: A new approach. *International Journal of Uncertainty, Fuzziness and Knowledge-based Systems* 14. (04): 445–459.
- AMINI, A. 1995. *Study of loess provenance and mechanisms of loess formation in Gharatikan watershed, Northeast Iran*. MSC thesis, Tehran, Tehran University. (in Persian)
- ARABAMERI, A., REZAEI, K., POURGHASEMI, H.R., LEE, S. and YAMANI, M. 2018. GIS-based gully erosion susceptibility mapping: a comparison among three data-driven models and AHP knowledge-based technique. *Environmental Earth Sciences* 77. (17): 1–22.
- ARABAMERI, A., CERDA, A., RODRIGO-COMINO, J., PRADHAN, B., SOHRABI, M., BLASCHKE, T. and TIEN BUI, D. 2019. Proposing a novel predictive technique for gully erosion susceptibility mapping in arid and semi-arid regions (Iran). *Remote Sensing* 11. (21): 2577.
- ASADI, S., MOORE, F. and KESHAVARZI, B. 2013. The nature and provenance of Golestan loess deposits in northeast Iran. *Geological Journal* 48. (6): 646–660. Available at <https://doi.org/10.1002/gj.2466>
- ASLAM, B., MAQSOOM, A., ALALLOUL, W.S., MUSARAT, M.A., JABBAR, T. and ZAFAR, A. 2021. Soil erosion susceptibility mapping using a GIS-based multi-criteria decision approach: Case of district Chitral, Pakistan. *Ain Shams Engineering Journal* 12. (2): 1637–1649.
- ASWATHI, J., SAJINKUMAR, K.S., RAJANEESH, A., OOMMEN, T., BOUALI, E.H., BINOJ KUMAR, R.B., RANI, V.R., THOMAS, J., THRIVIKRAMJI, K.P., AJIN, R.S. and ABIQUI, M. 2022. Furthering the precision of RUSLE soil erosion with PSInSAR data: An innovative model. *Geocarto International* 37. (27): 16108–16131. Available at <https://doi.org/10.1080/10106049.2022.2105407>
- AZAREH, A., RAHMATI, O., RAFIEI-SARDOOI, E., SANKEY, J.B., LEE, S., SHAHABI, H. and AHMAD, B.B. 2019. Modelling gully-erosion susceptibility in a semi-arid region, Iran: Investigation of applicability of certainty factor and maximum entropy models. *Science of the Total Environment* 655. 684–696.
- BARBERA, V., POMA, I., CRISTINA, L., NOVARA, A. and EGLI, M. 2012. Long-term cropping systems and tillage management effects on soil organic carbon stock and steady state level of C sequestration rates in a semiarid environment. *Land Degradation & Development* 23. (1): 82–91. Available at <https://doi.org/10.1002/ldr.1055>
- BELKENDIL, A., HABI, M., BOUTKHLIL, M., BOUZOUINA, O. and BOUFELDJA, S. 2018. Using multi-criteria evaluation (MCE): Analytical Hierarchy Process (AHP) in investigation of erosion phenomenon in arid zones. (Case study: Watershed of Bechar, southwest of Algeria). *Commission Scientifique / Scientific Committee* 18. 99–117.

- BELLOULA, M., DRIDI, H. and KALLA, M. 2020. Spatialization of water erosion using analytic hierarchy process (AHP) method in the high valley of the Medjerda, eastern Algeria. *Journal of Water and Land Development* 44. 19–25. Available at <https://doi.org/10.24425/jwld.2019.127041>
- BENISTON, J.W., SHIPITALO, M.J., LAL, R., DAYTON, E.A., HOPKINS, D.W., JONES, F., JOYNES, A. and DUNGAIT, J.A.J. 2015. Carbon and macronutrient losses during accelerated erosion under different tillage and residue management. *European Journal of Soil Science* 66. (1): 218–225. Available at <https://doi.org/10.1111/ejss.12205>
- BHATTACHARYA, R.K., CHATTERJEE, N.D. and DAS, K. 2020. Sub-basin prioritization for assessment of soil erosion susceptibility in Kangsabati, a plateau basin: A comparison between MCDM and SWAT models. *Science of the Total Environment* 734. 139474. Available at <https://doi.org/10.1016/j.scitotenv.2020.139474>
- BOUAMRANE, A., BOUAMRANE, A. and ABIDA, H. 2021. Water erosion hazard distribution under a semi-arid climate condition: Case of Mellah watershed, north-eastern Algeria. *Geoderma* 403. 115381. Available at <https://doi.org/10.1016/j.geoderma.2021.115381>
- BOUFELDJA, S., BABA HAMED, K., BOUANANI, A. and BELKENDIL, A. 2020. Identification of zones at risk of erosion by the combination of a digital model and the method of multi-criteria analysis in the arid regions: case of the Bechar Wadi watershed. *Applied Water Science* 10. (5): 121. Available at <https://doi.org/10.1007/s13201-020-01191-6>
- BOZALI, N. 2020. Assessment of the soil protection function of forest ecosystems using GIS-based Multi-Criteria Decision Analysis: A case study in Adiyaman, Turkey. *Global Ecology and Conservation* 24. e01271. Available at <https://doi.org/10.1016/j.gecco.2020.e01271>
- CEN, Y., ZHANG, B., LUO, J., DENG, Q., LIU, H. and WANG, L. 2022. Influence of topographic factors on the characteristics of gully systems in mountainous areas of Ningnan Dry-Hot Valley, SW China. *International Journal of Environmental Research and Public Health* 19. (14): 8784. Available at <https://doi.org/10.3390/ijerph19148784>
- COSTA, C.A.B. and VANSNICK, J.-C. 2008. A critical analysis of the eigenvalue method used to derive priorities in AHP. *European Journal of Operational Research* 187. (3): 1422–1428. Available at <https://doi.org/10.1016/j.ejor.2006.09.022>
- DAS, B., BORDOLOI, R., THUNGNON, L.T., PAUL, A., PANDEY, P.K., MISHRA, M. and TRIPATHI, O.P. 2020. An integrated approach of GIS, RUSLE and AHP to model soil erosion in West Kameng watershed, Arunachal Pradesh. *Journal of Earth System Science* 129. (1): 94. Available at <https://doi.org/10.1007/s12040-020-1356-6>
- DURLEVIĆ, U., VALJAREVIĆ, A., NOVKOVIĆ, I., ČURČIĆ, N.B., SMILJIĆ, M., MORAR, C., STOICA, A., BARIŠIĆ, D. and LUKIĆ, T. 2022. GIS-based spatial modelling of snow avalanches using analytic hierarchy process: A case study of the Šar Mountains, Serbia. *Atmosphere* 13. (8): 1229. Available at <https://doi.org/10.3390/atmos13081229>
- EBHUOMA, O., GEBRESLASIE, M., NGETAR, N.S., PHINZI, K. and BHATTACHARJEE, S. 2022. Soil erosion vulnerability mapping in selected rural communities of uThukela catchment, South Africa, using the analytic hierarchy process. *Earth Systems and Environment* 6. (4): 851–864.
- ECHOGDALI, F.Z., BOUTALEB, S., TAIA, S., OUCHCHEN, M., ID-BELQAS, M., KPAN, R.B., ABILOU, M., ASWATHI, J. and SAJINKUMAR, K.S. 2022. Assessment of soil erosion risk in a semi-arid climate watershed using SWAT model: Case of Tata basin, South-East of Morocco. *Applied Water Science* 12. (6): 137. Available at <https://doi.org/10.1007/s13201-022-01664-w>
- EL JAZOULI, A., BARAKAT, A. and KHELLOUK, R. 2019. GIS-multicriteria evaluation using AHP for landslide susceptibility mapping in Oum Er Rbia high basin (Morocco). *Geoenvironmental Disasters* 6. (3): 1–12. Available at <https://doi.org/10.1186/s40677-019-0119-7>
- EMERSON, W.W. and MCGARRY, D. 2003. Organic carbon and soil porosity. *Soil Research* 41. (1): 107–118. Available at <https://doi.org/10.1071/SR01064>
- ENNAJI, N., OUAKHIR, H., HALOUAN, S. and ABAHROUR, M. 2022. Assessment of soil erosion rate using the EPM model: Case of Ououmana basin, Middle Atlas, Morocco. *IOP Conference Series: Earth and Environmental Science* 1090. (1): 012004. Available at <https://doi.org/10.1088/1755-1315/1090/1/012004>
- FARAH, A., ALGOUTI, A., ALGOUTI, A., IFKIRNE, M. and EZZIYANI, A. 2021. Mapping of soil degradation in semi-arid environments in the ouarazate basin in the south of the central High Atlas, Morocco, using sentinel 2A data. *Remote Sensing Applications: Society and Environment* 23. 100548. Available at <https://doi.org/10.1016/j.rsase.2021.100548>
- FEIZI, V., AZIZI, G., ALIMOHAMMADIAN, H. and MOLLASHAHI, M. 2023. Magnetic properties and geochemistry of loess/paleosol sequences at Nowdeh section northeastern of Iran. *Climate of the Past, Discuss.* 2023-56. 1–14. Available at <https://doi.org/10.5194/cp-2023-56>
- FEIZIZADEH, B., SHADMAN ROODPOSHTI, M., JANKOWSKI, P. and BLASCHKE, T. 2014. A GIS-based extended fuzzy multi-criteria evaluation for landslide susceptibility mapping. *Computers & Geosciences* 73. 208–221. Available at <https://doi.org/10.1016/j.cageo.2014.08.001>
- FENN, K., MILLAR, I.L., DURCAN, J.A., THOMAS, D.S.G., BANAK, A., MARKOVIĆ, S.B., VERES, D. and STEVENS, T. 2022. The provenance of Danubian loess. *Earth-Science Reviews* 226. 103920. Available at <https://doi.org/10.1016/j.earscirev.2022.103920>

- FRECHEN, M., KEHL, M., ROLF, C., SARVATI, R. and SKOWRONEK, A. 2009. Loess chronology of the Caspian Lowland in Northern Iran. *Quaternary International* 198. (1): 220–233. Available at <https://doi.org/10.1016/j.quaint.2008.12.012>
- GHAFFARPOUR, A., KHORMALI, F., BALSAM, W., KARIMI, A. and AYOUBI, S. 2016. Climatic interpretation of loess-paleosol sequences at Mobarakabad and Aghband, Northern Iran. *Quaternary Research* 86. (1): 95–109. Available at <https://doi.org/10.1016/j.yqres.2016.05.004>
- GHAFFARPOUR, A., KHORMALI, F., TAZIKEH, H., KEHL, M., ROLF, C., FRECHEN, M. and ZEEDEN, C. 2023. Geophysical sediment properties of a late Pleistocene loess-paleosol sequence, Chenarli, northeastern Iran. *Quaternary Research* 114. 114–129. Available at <https://doi.org/10.1017/qua.2023.5>
- GHAHRAMAN, K. and NAGY, B. 2023. Flood risk on arid alluvial fans: a case study in the Joghatay Mountains, northeast Iran. *Journal of Mountain Science* 20. (5): 1183–1200. Available at <https://doi.org/10.1007/s11629-022-7635-8>
- GHARIBREZA, M., ZAMAN, M., PORTO, P., FULAJTAR, E., PARSAEI, L. and EISAEI, H. 2020. Assessment of deforestation impact on soil erosion in loess formation using ¹³⁷Cs method (case study: Golestan Province, Iran). *International Soil and Water Conservation Research* 8. (4): 393–405. Available at <https://doi.org/10.1016/j.iswcr.2020.07.006>
- GÓMEZ-GUTIÉRREZ, Á., CONOSCENTI, C., ANGLIERI, S.E., ROTIGLIANO, E. and SCHNABEL, S. 2015. Using topographical attributes to evaluate gully erosion proneness (susceptibility) in two mediterranean basins: Advantages and limitations. *Natural Hazards* 79. (1): 291–314.
- HARRIS, H.L. and DREW, W.B. 1943. On the establishment and growth of certain legumes on eroded and uneroded sites. *Ecology* 24. (2): 135–148.
- HAYATZADEH, M., MOOSAVI, V. and ALIRAMAEI, R. 2023. Assessment and prioritization of soil erosion triggering factors using analytical hierarchy process and Taguchi method. *International Journal of Sediment Research* 38. (3): 396–404. Available at <https://doi.org/10.1016/j.ijsrc.2022.11.002>
- HUANG, C., HOU, X. and LI, H. 2022. An improved minimum cumulative resistance model for risk assessment of agricultural non-point source pollution in the coastal zone. *Environmental Pollution* 312. 120036. Available at <https://doi.org/10.1016/j.envpol.2022.120036>
- JAAFARI, A., NAJAFI, A., POURGHASEMI, H., REZAEIAN, J. and SATTARIAN, A. 2014. GIS-based frequency ratio and index of entropy models for landslide susceptibility assessment in the Caspian forest, northern Iran. *International Journal of Environmental Science and Technology* 11. (4): 909–926.
- JEBUR, M.N., PRADHAN, B. and TEHRANY, M.S. 2014. Optimization of landslide conditioning factors using very high-resolution airborne laser scanning (LIDAR) data at catchment scale. *Remote Sensing of Environment* 152. 150–165.
- KACHOURI, S., ACHOUR, H., ABIDA, H. and BOUAZIZ, S. 2015. Soil erosion hazard mapping using Analytic Hierarchy Process and logistic regression: A case study of Haffouz watershed, central Tunisia. *Arabian Journal of Geosciences* 8. (6): 4257–4268.
- KAHSAY, A., HAILE, M., GEBRESAMUEL, G. and MOHAMMED, M. 2018. Land suitability analysis for sorghum crop production in northern semi-arid Ethiopia: Application of GIS-based fuzzy AHP approach. *Cogent Food & Agriculture* 4. (1): 1507184. Available at <https://doi.org/10.1080/23311932.2018.1507184>
- KARIMI, A., FRECHEN, M., KHADEMI, H., KEHL, M. and JALALIAN, A. 2011. Chronostratigraphy of loess deposits in northeast Iran. *Quaternary International* 234. (1–2): 124–132.
- KEBEDE, Y.S., ENDALAMAW, N.T., SINSHAW, B.G. and ATINKUT, H.B. 2021. Modelling soil erosion using RUSLE and GIS at watershed level in the Upper Beles, Ethiopia. *Environmental Challenges* 2. 100009. Available at <https://doi.org/10.1016/j.envc.2020.100009>
- KEHL, M., VLAMINCK, S., KÖHLER, T., LAAG, C., ROLF, C., TSUKAMOTO, S., FRECHEN, M., SUMITA, M., SCHMINCKE, H.-U. and KHORMALI, F. 2021. Pleistocene dynamics of dust accumulation and soil formation in the southern Caspian Lowlands – New insights from the loess-paleosol sequence at Neka-Abelou, northern Iran. *Quaternary Science Reviews* 253. 106774. Available at <https://doi.org/10.1016/j.quascirev.2020.106774>
- KHORMALI, F., AJAMI, M., AYOUBI, S., SRINIVASARAO, C. and WANI, S.P. 2009. Role of deforestation and hillslope position on soil quality attributes of loess-derived soils in Golestan province, Iran. *Agriculture, Ecosystems & Environment* 134. (3): 178–189. Available at <https://doi.org/10.1016/j.agee.2009.06.017>
- KÖPPEN, W. 1900. Versuch einer Klassifikation der Klimate, vorzugsweise nach ihren Beziehungen zur Pflanzenwelt. (Schluss). *Geographische Zeitschrift* 6. (12): 657–679. Available at <http://www.jstor.org/stable/27803939>
- KUCUKER, D.M. and GIRALDO, D.C. 2022. Assessment of soil erosion risk using an integrated approach of GIS and Analytic Hierarchy Process (AHP) in Erzurum, Türkiye. *Ecological Informatics* 71. 101788.
- LE ROUX, J.J. and SUMNER, P. 2012. Factors controlling gully development: comparing continuous and discontinuous gullies. *Land Degradation & Development* 23. (5): 440–449.
- LI, Y., JIANG, Z., CHEN, Z., YU, Y., LAN, F., SHAN, Z., SUN, Y., LIU, P., TANG, X. and RODRIGO-COMINO, J. 2020. Anthropogenic disturbances and precipitation affect karst sediment discharge in the Nandong

- underground river system in Yunnan, Southwest China. *Sustainability* 12. (7). 3006. Available at <https://doi.org/10.3390/su12073006>
- LUKIĆ, T., LEŠČEŠEN, I., SAKULSKI, D., BASARIN, B. and JORDAAN, A. 2016. Rainfall erosivity as an indicator of sliding occurrence along the southern slopes of the Bačka loess plateau: a case study of the Kula settlement, Vojvodina (North Serbia). *Carpathian Journal of Earth and Environmental Sciences* 11. (2): 303–318.
- LUKIĆ, T., BJELAJAC, D., FITZSIMMONS, K.E., MARKOVIĆ, S.B., BASARIN, B., MLADAN, D., MICIC, T., SCHÄTZL, R.J., GAVRILOV, M.B. and MILANOVIĆ, M. 2018. Factors triggering landslide occurrence on the Zemun loess plateau, Belgrade area, Serbia. *Environmental Earth Sciences* 77. 13. Available at <https://doi.org/10.1007/s12665-018-7712-z>
- LUKIĆ, T., LUKIĆ, A., BASARIN, B., PONJIGER, T.M., BLAGOJEVIĆ, D., MEŠAROŠ, M., MILANOVIĆ, M., GAVRILOV, M., PAVIĆ, D., ZORN, M., KOMAC, B., MILJKOVIĆ, Đ., SAKULSKI, D., BABIĆ-KEKEZ, S., MORAR, C. and JANIĆEVIĆ, S. 2019. Rainfall erosivity and extreme precipitation in the Pannonian basin. *Open Geosciences* 11. (1): 664–681. Available at <https://doi.org/doi:10.1515/geo-2019-0053> (Open Geosciences)
- MARKOVIĆ, S.B., TIMAR-GABOR, A., STEVENS, T., HAMBACH, U., POPOV, D., TOMIĆ, N., OBREHT, I., JOVANOVIĆ, M., LEHMKUHL, F., KELS, H., MARKOVIĆ, R. and GAVRILOV, M.B. 2014. Environmental dynamics and luminescence chronology from the Orlovat loess–palaeosol sequence (Vojvodina, northern Serbia). *Journal of Quaternary Science* 29. (2): 189–199. Available at <https://doi.org/10.1002/jqs.2693>
- MESHAM, S.G., SINGH, V.P., KAHYA, E., SEPEHRI, M., MESHAM, C., HASAN, M.A., ISLAM, S. and DUC, P.A. 2022. Assessing erosion prone areas in a watershed using interval rough-analytical hierarchy process (IR-AHP) and fuzzy logic (FL). *Stochastic Environmental Research and Risk Assessment* 36. (2): 297–312. Available at <https://doi.org/10.1007/s00477-021-02134-6>
- MICIĆ PONJIGER, T., LUKIĆ, T., WILBY, R.L., MARKOVIĆ, S.B., VALJAREVIĆ, A., DRAGIĆEVIĆ, S., GAVRILOV, M.B., PONJIGER, I., DURLEVIĆ, U., MILANOVIĆ, M.M., BASARIN, B., MLADAN, D., MITROVIĆ, N., GRAMA, V. and MORAR, C. 2023. Evaluation of rainfall erosivity in the Western Balkans by mapping and clustering ERA5 reanalysis data. *Atmosphere* 14. (1): 104. Available at <https://doi.org/10.3390/atmos14010104>
- MORGAN, R. 1995. *Soil Erosion and Conservation*. London, Longman.
- MORGAN, R., QUINTON, J., SMITH, R., GOVERS, G., POESEN, J., AUERSWALD, K., CHISCI, G., TORRI, D. and STYCZEN, M. 1998. The European Soil Erosion Model (EUROSEM): A dynamic approach for predicting sediment transport from fields and small catchments. *Earth Surface Processes and Landforms: The Journal of the British Geomorphological Group* 23. (6): 527–544.
- MUHS, D.R. 2007. Loess deposits, origins and properties. In *Encyclopedia of Quaternary Science*. Eds.: SCOTT, E.A. and MCKE, C.J., Elsevier, 1405–1418. Available at <https://doi.org/10.1016/B0-44-452747-8/00158-7>
- MUSHTAQ, F., FAROOQ, M., TIRKEY, A.S. and SHEIKH, B.A. 2023. Analytic hierarchy process (AHP) based soil erosion susceptibility mapping in northwestern Himalayas: A case study of Central Kashmir province. *Conservation* 3. (1): 32–52. Available at <https://doi.org/10.3390/conservation3010003>
- NEITSCH, S.L., ARNOLD, J.G., KINIRY, J.R. and WILLIAMS, J.R. 2011. *Soil and water assessment tool theoretical documentation*. Version 2009. Temple, TX, USA, Blackland Research Center.
- NEJI, N., AYED, R.B. and ABIDA, H. 2021. Water erosion hazard mapping using analytic hierarchy process (AHP) and fuzzy logic modeling: a case study of the Chaffar Watershed (Southeastern Tunisia). *Arabian Journal of Geosciences* 14. (13): 1–15.
- OKHRAVI, R. and AMINI, A. 2001. Characteristics and provenance of the loess deposits of the Gharatikan watershed in northeast Iran. *Global and Planetary Change* 28. (1–4): 11–22.
- OLII, M.R., OLII, A., PAKAYA, R. and OLII, M.Y.U.P. 2023. GIS-based analytic hierarchy process (AHP) for soil erosion-prone areas mapping in the Bone Watershed, Gorontalo, Indonesia. *Environmental Earth Sciences* 82. (9): 225. Available at <https://doi.org/10.1007/s12665-023-10913-3>
- PANDEY, S., KUMAR, P., ZLATIC, M., NAUTIYAL, R. and PANWAR, V.P. 2021. Recent advances in assessment of soil erosion vulnerability in a watershed. *International Soil and Water Conservation Research* 9. (3): 305–318. Available at <https://doi.org/10.1016/j.iswcr.2021.03.001>
- PARSIAN, S., AMANI, M., MOGHIMI, A., GHORBANIAN, A. and MAHDAVI, S. 2021. Flood hazard mapping using fuzzy logic, analytical hierarchy process, and multi-source geospatial datasets. *Remote Sensing* 13. (23): 4761. Available at <https://doi.org/10.3390/rs13234761>
- PÉCSI, M. 1990. Loess is not just the accumulation of dust. *Quaternary International* 7. 1–21.
- PHINZI, K., NGETAR, N.S. and EBHUOMA, O. 2021. Soil erosion risk assessment in the Umzintlava catchment (T32E), Eastern Cape, South Africa, using RUSLE and random forest algorithm. *South African Geographical Journal* 103. (2): 139–162.
- PYE, K. and TSOAR, H. 1987. The mechanics and geological implications of dust transport and deposition in deserts with particular reference to loess formation and dune sand diagenesis in the northern Negev, Israel. *Geological Society, London, Special Publications* 35. (1): 139–156.
- RAHMATI, O., HAGHIZADEH, A., POURGHASEMI, H.R. and NOORMOHAMADI, F. 2016. Gully erosion susceptibility mapping: The role of GIS-based bivariate

- statistical models and their comparison. *Natural hazards* 82. (2): 1231–1258.
- RAHMATI, O., TAHMASEBPOUR, N., HAGHIZADEH, A., POURGHASEMI, H.R. and FEIZIZADEH, B. 2017. Evaluating the influence of geo-environmental factors on gully erosion in a semi-arid region of Iran: An integrated framework. *Science of the Total Environment* 579. 913–927.
- RAJESH, C., DIBYENDU, D., RABINDRA, N.B. and UTTAM, K.M. 2016. Analytic hierarchy process and multi-criteria decision-making approach for selecting the most effective soil erosion zone in Gomati river basin. *International Journal of Engineering Research & Technology* 5. (1): 595–600. Available at <https://doi.org/10.17577/IJERTV5IS010474>
- RAZA, A., AHRENDTS, H., HABIB-UR-RAHMAN, M. and GAISER, T. 2021. Modeling approaches to assess soil erosion by water at the field scale with special emphasis on heterogeneity of soils and crops. *Land* 10. (4): 422. Available at <https://doi.org/10.3390/land10040422>
- RICHTHOFEN, F. 1872. Reisen im nördlichen China: Ueber den chinesischen Löss. *Verhandlungen der Kaiserlich-Königlichen geologischen Reichsanstalt* 8. 153–160.
- SAATY, R.W. 1987. The analytic hierarchy process – what it is and how it is used? *Mathematical Modelling* 9. (3–5): 161–176.
- SAATY, T.L. 1980. *The Analytic Hierarchy Process*. New York, McGraw Hill.
- SAATY, T.L. 1988. What is the analytic hierarchy process? In *Mathematical Models for Decision Support*. Eds.: MITRA, G., GREENBERG, H.J., LOOTSMA, F.A., RIJKAERT, M.J. and ZIMMERMANN, H.J., Cham, Springer, 109–121.
- SAATY, T.L. and VARGAS, L.G. 2001. How to make a decision. In *Models, Methods, Concepts & Applications of the Analytic Hierarchy Process*. New York, Springer, 1–25.
- SAHA, S., GAYEN, A., POURGHASEMI, H.R. and TIEFENBACHER, J.P. 2019. Identification of soil erosion-susceptible areas using fuzzy logic and analytical hierarchy process modeling in an agricultural watershed of Burdwan district, India. *Environmental Earth Sciences* 78. (23): 1–18.
- SAINI, S.S., JANGRA, R. and KAUSHIK, S. 2015. Vulnerability assessment of soil erosion using geospatial techniques: A pilot study of upper catchment of Markanda river. *International Journal of Advancement in Remote Sensing, GIS and Geography* 2. (1): 9–21.
- SANDEEP, P., REDDY, G.P.O., JEGANKUMAR, R. and ARUN KUMAR, K.C. 2021. Modeling and assessment of land degradation vulnerability in semi-arid ecosystem of southern India using temporal satellite data, AHP and GIS. *Environmental Modeling & Assessment* 26. (2): 143–154. Available at <https://doi.org/10.1007/s10666-020-09739-1>
- SHAHABI, H. and HASHIM, M. 2015. Landslide susceptibility mapping using GIS-based statistical models and remote sensing data in tropical environment. *Scientific Reports* 5. (1): 9899.
- SHARIFIGARMDAREH, J., KHORMALI, F., SCHEIDT, S., ROLF, C., KEHL, M. and FRECHEN, M. 2020. Investigating soil magnetic properties with pedogenic variation along a precipitation gradient in loess-derived soils of the Golestan province, northern Iran. *Quaternary International* 552. 100–110. Available at <https://doi.org/10.1016/j.quaint.2019.11.022>
- SHEN, N., WANG, Z., ZHANG, F. and ZHOU, C. 2023. Response of soil detachment rate to sediment load and model examination: A key process simulation of rill erosion on steep loessial hillslopes. *International Journal of Environmental Research and Public Health* 20. (4): 2839. Available at <https://doi.org/10.3390/ijerph20042839>
- SINSHAW, B.G., BELETE, A.M., TEFERA, A.K., DESSIE, A.B., BIZUNEH, B.B., ALEM, H.T., ATANAW, S.B., ESHETE, D.G., WUBETU, T.G., ATINKUT, H.B. and MOGES, M.A. 2021. Prioritization of potential soil erosion susceptibility region using fuzzy logic and analytical hierarchy process, upper Blue Nile Basin, Ethiopia. *Water-Energy Nexus* 4. 10–24. Available at <https://doi.org/10.1016/j.wen.2021.01.001>
- SMALLEY, I., MARKOVIĆ, S.B. and SVIRČEV, Z. 2011. Loess is [almost totally formed by] the accumulation of dust. *Quaternary International* 240. (1–2): 4–11.
- TAIRI, A., ELMOUDEN, A. and ABOULOFAFA, M. 2019. Soil erosion risk mapping using the analytical hierarchy process (AHP) and geographic information system in the tifnout-askaoun watershed, southern Morocco. *European Scientific Journal* 15. (30): 1857–1743.
- THOMAS, J., JOSEPH, S. and THRIVIKRAMJI, K. 2018. Assessment of soil erosion in a tropical mountain river basin of the southern Western Ghats, India using RUSLE and GIS. *Geoscience Frontiers* 9. (3): 893–906.
- VANMAERCKE, M., PANAGOS, P., VANWALLEGHEM, T., HAYAS, A., FOERSTER, S., BORRELLI, P., ROSSI, M., TORRI, D., CASALI, J., BORSELLI, L., VIGIAK, O., MAERKER, M., HAREGEWEYN, N., DE GEETER, S., ZGLOBICKI, W., BIELDERS, C., CERDÀ, A., CONOSCENTI, C., DE FIGUEIREDO, T., EVANS, B., GOLOSOV, V., IONITA, I., KARYDAS, C.G., KERTÉSZ, Á., KRASA, J., LE BOUTELLIER, C., RADOANE, M., RISTIC, R., ROUSSEVA, S., STANKOVIANSKY, M., STOLTE, J., STOLZ, C., BARTLEY, R., WILKINSON, S., JARIBAH, B. and POESEN, J. 2021. Measuring, modelling and managing gully erosion at large scales: A state of the art. *Earth-Science Reviews* 218. 103637. Available at <https://doi.org/10.1016/j.earscirev.2021.103637>
- WANG, X., JIAO, F., LI, X. and AN, S. 2017. The Loess Plateau. In *Multifunctional Land-Use Systems for Managing the Nexus of Environmental Resources*. Eds.: ZHANG, L. and SCHWÄRZEL, K., Cham, Springer, 11–27. Available at https://doi.org/10.1007/978-3-319-54957-6_2

- WU, Q., JIA, C., CHEN, S. and LI, H. 2019. SBAS-InSAR based deformation detection of urban land, created from mega-scale mountain excavating and valley filling in the Loess Plateau: The case study of Yan'an city. *Remote Sensing* 11. (14): 1673. Available <https://doi.org/10.3390/rs11141673>
- XU, J., WU, Z., CHEN, H., SHAO, L., ZHOU, X. and WANG, S. 2022. Influence of dry-wet cycles on the strength behavior of basalt-fiber reinforced loess. *Engineering Geology* 302. 106645. Available at <https://doi.org/10.1016/j.enggeo.2022.106645>
- YOUNG, R., ONSTAD, C., BOSCH, D. and ANDERSON, W. 1989. AGNPS: A nonpoint-source pollution model for evaluating agricultural watersheds. *Journal of Soil and Water Conservation* 44. (2): 168–173.
- ZHANG, J., YANG, M., DENG, X., LIU, Z., and ZHANG, F. 2019. The effects of tillage on sheet erosion on sloping fields in the wind-water erosion crisscross region of the Chinese Loess Plateau. *Soil and Tillage Research* 187. 235–245. Available at <https://doi.org/10.1016/j.still.2018.12.014>
- ZHAO, J., VANMAERCKE, M., CHEN, L. and GOVERS, G. 2016. Vegetation cover and topography rather than human disturbance control gully density and sediment production on the Chinese Loess Plateau. *Geomorphology* 274. 92–105.
- ZHU, K.-W., CHEN, Y.-C., ZHANG, S., YANG, Z.-M., HUANG, L., LI, L., LEI, B., ZHOU, Z.-B., XIONG, H.-L., LI, X.-X., LI, Y.-C. and ISLAM, S. 2020. Output risk evolution analysis of agricultural non-point source pollution under different scenarios based on multi-model. *Global Ecology and Conservation* 23. e01144. Available at <https://doi.org/10.1016/j.gecco.2020.e01144>
- ZOU, L., LIU, Y., WANG, Y. and HU, X. 2020. Assessment and analysis of agricultural non-point source pollution loads in China: 1978–2017. *Journal of Environmental Management* 263. 110400. Available at <https://doi.org/10.1016/j.jenvman.2020.110400>